Applied Catalysis B: Environmental 304 (2022) 120962

Contents lists available at ScienceDirect

Applied Catalysis B: Environmental

journal homepage: www.elsevier.com/locate/apcatb

Trap efficiency of exhaust gas pollutants in microporous sorbents under representative driving conditions

K. Barbera-Italiano [a,*], E. Jeudy [a], M. Lecompte [a], E. Laigle [b], C. Norsic [b], C. Chaillou [b], G. Bourhis [c]

[a] IFP Energies nouvelles, Rond-point de l'échangeur de Solaize, Institut Carnot IFPEN Transports Energie, BP 3, 69360 Solaize, France
[b] Aramco Fuel Research Center, 232 Avenue Bonaparte, Rueil-Malmaison 92852, France
[c] IFP Energies nouvelles, Institut Carnot IFPEN Transports Energie, 1 et 4 avenue de Bois-Préau, 92852 Rueil-Malmaison Cedex, France

ARTICLE INFO

Keywords:
Activated carbon
Zeolites
Adsorption
Exhaust gas
Hydrocarbon speciation
Emission vehicle control

ABSTRACT

The objective of this study is to develop a Neutral Air Quality Impact Vehicle (NAQIV) using a system able to reduce the tailpipe emissions of a gasoline powertrain engine. A possible configuration is a bypass in the exhaust, close to the tailpipe, that stores pollutants during the cold start phase when most emissions occur. For this purpose, adsorption efficiencies of commercial sieved powders Activated Carbon (AC), and zeolites (BEA, MFI) were screened at trap temperatures of 25, 50, and 150 °C using two different exhaust gas compositions. These compositions are obtained from two different phases of the World Harmonized Light-Duty Test Cycle (WLTC): the first 100 s after the engine start, and the first "5 km" after a cold start, the latter being representative of typical emissions of an automotive vehicle on an average trip in urban areas. The aim is also to provide sorption capacity not only in respect to the conventional pollutants (CO, NO_x, CO_2), and the most common NMHCs present in the exhaust gas (toluene, i-pentane, n-pentane, acetylene, ethylene, and methane), but also towards unregulated pollutants such as NH_3, CH_4 and N_2O (to be introduced in Euro 7 regulations). The experimental results reveal a superior performance of AC NMHCs adsorption (and particularly toluene, n-pentane and i-pentane) which is not affected by the presence of other pollutants, but is negatively impacted by rising temperature and flow gas composition. Among zeolites, only Cu/Beta and Cu/ZSM-5 display moderate adsorption capacity of NH_3, NMHCs and NO. In particular, the adsorption of ethylene and acetylene over Cu/ZSM-5 is strongly promoted at lower H_2O concentrations. Finally, desorption profiles of each pollutant were generated through Temperature Programmed Desorption (TPD) experiments, unraveling sorbate-sorbent interactions.

1. Introduction

Although the transportation sector is progressively decarbonizing, emissions mitigation solutions are still required to reduce the environmental impact of automotive fuel combustion. The future Euro 7 guidelines will impose more severe regulations to achieve Clean Air -to which Non Methanic Hydrocarbons (NMHC), NO_X, NH_3, CO and Particulate Matter (PM) negatively contribute-, Energy Efficiency and Greenhouse Gases (CO_2, NO_x, CH_4, N_2O) abatement. The guidelines aim to promote the development of a near zero impact emission technology with a neutral or positive effect on urban Air Quality [1] whether for conventional gasoline engines or hybrid vehicles. Indeed, exhaust gas composition is strongly engine and temperature dependent, requiring tailor-made after treatment systems for emissions control [2,3].

A promising strategy to address this variability consists in developing $N_xH_yO_z$/VOC/CO sorption/purification technologies [4] coupled with a second catalytic After-Treatment System (ATS), such as a SCR or Three Way Catalysts (TWC) [5,6]. The majority of the exhaust pollutants are emitted during the very first seconds of a cold start, during which the engine operates under non stoichiometric and non-optimal (i.e. injection and spark timing) conditions to achieve high exhaust thermal conditions, combustion stability and vehicle drivability. Pollutants are released in the atmosphere until the ATS reaches its operative light-off temperature, i.e. typically 200–300 °C [7]. Reducing cold-start emissions requires such approaches as a reduction of the engine-out pollutant level (by increasing gas exhaust temperatures), quicker catalyst light-off

* Corresponding author.
E-mail addresses: katia.barbera-italiano@ifpen.fr (K. Barbera-Italiano), Christophe.Chaillou@aramcooverseas.com (C. Chaillou), guillaume.bourhis@ifpen.fr (G. Bourhis).

https://doi.org/10.1016/j.apcatb.2021.120962
Received 16 July 2021; Received in revised form 22 November 2021; Accepted 22 November 2021
Available online 29 November 2021

Scheme 1. Schematic illustration of all the possible configuration implying the use of a sorbent upstream or downstream an ATS.

(by use of electrical heater) [8] and the adoption of a cold trap system upstream the ATS, such as zeolites [9]. This latter can provide a gradual desorption of pollutants from sorbent at higher temperatures following the light-off of the catalyst. Nevertheless, the sorbent should not slow down the heating up of the ATS through preferential capture of sensible and/or adsorption enthalpy of exhaust gas [10]. Alternatively sorbents can be located downstream the ATS to trap the unconverted pollutants. In this case, a recirculation loop might be needed in the exhaust line in order to convert desorbed pollutants as the temperature increases. In all cases, a bypass of the sorbents is needed to prevent their deterioration by exposure to high temperature exhaust gases. It is important to point out that, due to the different scope of the sorbent and the ATS, the criteria for the choice of a proper sorbent may be different to that for the ATS itself. As an example, whilst a Cu/base zeolite may present many advantages as a sorbent [11], it would be sub-optimal as catalytic converter [12].

Meeting all these requirements simultaneously is quite challenging and the basic processes governing the trapping of complex mixtures in absence/presence of inhibitors in relation with the diffusive and chemical properties of sorbents are poorly understood [13].

Sorption based purification processes require sorbents with high efficiency both in adsorption and containment of pollutants, and tolerance to a variety of feeds. Furthermore, periodic thermal regeneration methods can result in sorbent restructuration/decomposition. For this purpose, two options are envisageable with a common initial step of opening the bypass to let the temperature heat the sorbents: i) to reinject the flow upstream of the ATS (which is now activated), or ii) to let the desorbed pollutants passing through an 'ozone part',where ozone reacts with the unconverted pollutants. All the possibilities are illustrated in Scheme 1.

The use of Activated Carbon is largely recognized as a valid alternative which can simultaneously remove pollutants and act as a catalyst. Indeed, a moving bed of Activated Carbon, sorbs in the presence of water starting from a very low temperature (25 °C). After a test, it can be fully regenerated by heating in an inert atmosphere without exceeding 600 °C.

Over the last few decades, other dedicated materials with a potential to adsorb and convert the different pollutants, have been reported in literature but their effective efficiency when considering pollutant cross-interactions has never been screened.The overall adsorption process is indeed much more complex than the single adsorption process, and sorbent optimization relies strongly on the control of elementary processes occurring under dynamic conditions.

This usually implies accounting for multicomponent gas mixtures, rapid warm up, fluctuations in space, velocity, temperature and gas concentrations. For this reason, the aim of this work is to provide a broad (but not fully extensive) overview of adsorption profiles and material behavior of commercial sorbents. A typical range of temperatures (encountered during a cold start), feed compositions and a case study representing the real cycle of a sorbent in a gasoline powertrain exhaust have been investigated. The aim is also to evaluate its capacity to adsorb not only the conventional pollutants (notably, CO, NO_x, HCs), coupled with the speciation of the most common HCs present in the exhaust gas, but also future Euro 7 regulated pollutants such as NH_3, N_2O and CH_4 (to be introduced in the limitations). This work thereby provides original data for model calibration and validation [14].

Table 1
Physical properties of the commercial sorbents under study.

Sorbents	SiO_2/Al_2O_3[a]	Pore size[a] (Å)	Metal loading[a] (wt%)	Specific S. A.[a] (m^2/g)	Particle size[a] (μm)
Cu/ZSM-5	30	~ 6	4.5	300 - 700	2–5
Cu/Beta	30	~ 7	4.5	500 - 800	2–5
AC	–	12	–	1514	210–595

[a] According to the producer.

2. Experimental

2.1. Material

Cu/ZSM-5, Cu/Beta, Fe/Beta and NH_4/Beta zeolites were provided by CLARIANT. No additional information about synthesis and characterization can be provided due to a confidentiality agreement with the producer. Activated Carbon was supplied by NORIT; the AC GCN3070 used was produced from coconut shell by using steam for physical activation. The basic physical and chemical properties approved for communication by the producers are listed in Table 1.

2.2. Tests on synthetic gas bench

The composition of the gasoline exhaust gas was determined from previous chassis dynamometer bench tests with a Gasoline Direct Injection (GDI) vehicle (Euro 6d temp). The World Harmonized Light-Duty Test Cycle (WLTC) with cold start at 20 °C was performed during these tests. The concentrations used in this study are presented in Table 2. Two different mixtures were tested for adsorption experiments: a mixture code named "cold start", corresponding to the average composition in the tailpipe over the first 100 s of the cycle, and a mixture representative of the average concentrations over a distance of 5 km (the first 5 km of a WLTC are typical of automotive trips in urban areas), code named "5 km" hereafter.

Experiments were carried out in a tubular flow quartz reactor under atmospheric pressure depicted in [14]. To operate at residence times representative of a typical ATS, a total flow rate of 4.94 NL/min of N_2 was first passed through 430 mg of sieved powder sorbent (200–355 μm) and then, after 120 s, the exhaust gas mixture is injected at the same GHSV. The temperature was controlled by two thermocouples placed upstream and downstream of the sorbent bed. All sorbents were tested at a trap temperature (T_{ads}) of 25 °C and under "cold start" first. Those with the best trap efficiencies were further tested at higher T_{ads} (50 °C and 150 °C) under "5 km" condition, until reaching saturation for each molecule of pollutant present in the gas stream. Once saturation was achieved, the sorbent was first flushed under N_2 flow of 4.94 NL/min, to ensure the purge of residual pollutants in the lines, before the Temperature Programmed Desorption (TPD) measurement in the T_{ads} – 600 °C range was run under the same N_2 flow at a heating rate of 5 or 10 °C/min. The adsorbed/desorbed stream composition was analyzed on-line with a 1 Hz resolution by IR laser (for CO_2, NO, NH_3, N_2O, H_2O), and a Non Dispersive-IR (for CO). The total amount of HCs was quantified by a Flame Ionization Detector coupled with a μGC INFICON to identify the adsorption/desorption of each hydrocarbon every 335 s. To quantify the setup error induced on the measurement (due to some possible concentration gradients within pipes, or

Table 2
Inlet compositions of the synthetic exhaust gas passing through the tubular flow reactor.

	Feed gas composition											
	ppmC						ppm				vol%	
	$n\text{-}C_5H_{12}$	$i\text{-}C_5H_{12}$	C_7H_8	C_2H_4	C_2H_2	CH_4	CO	NO	N_2O	NH_3	CO_2	H_2O
"Cold start" mixture	500	250	350	400	40	75	3000	75	10	50	10	1,5
"5 km" mixture	100	50	70	80	8	15	750	20	5	20	10	5

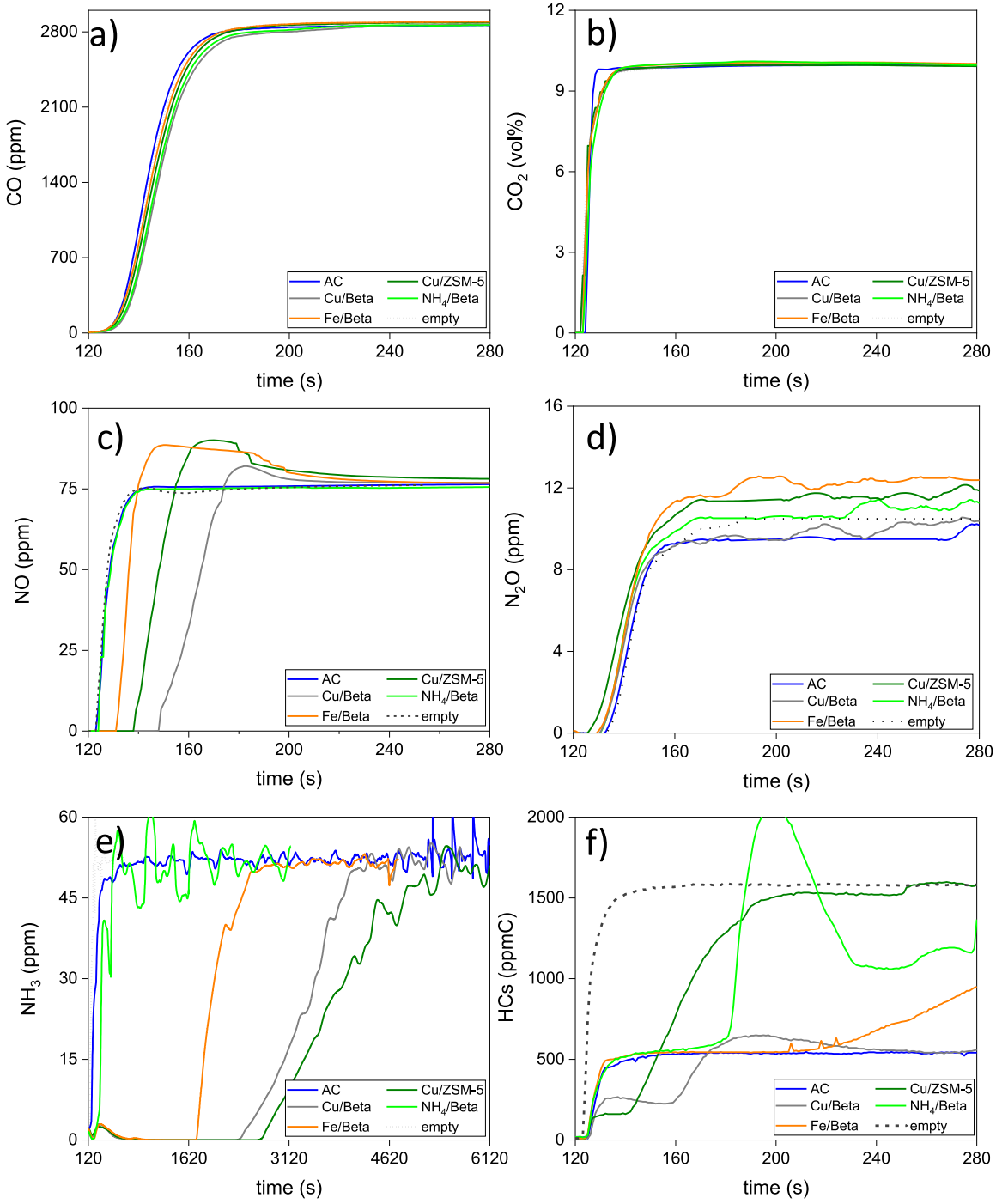

Fig. 1. Breakthrough curves obtained with time on stream over all materials (NH_4/Beta, Cu/ZSM-5, Fe/Beta, Cu/Beta, AC) under constant adsorption conditions – "cold start" mixture and $T_{25\,°C}$.

Table 3
Comparison of quantitative uptake (ads) and release (des) among the most active sorbents, under "cold start" at $T_{25\,°C}$, and "5 km" (5 times more dilutes) at $T_{50\,°C}$ and $T_{150\,°C}$, respectively.

Sample	T_{ads}-mixture	NH_3[a]		HCs[a]		NO[a]	
		ads	*des*[b]	*ads*	*des*[b]	*ads*	*des*[b]
AC	25 °C -cold start	54	55	6461	5778	11	7.4
	50 °C - 5 km	23	14	2683	3107	6	5.5
	150 °C - 5 km	21	23	426	445	6	0.5
Cu/Beta	25 °C - cold start	1492	N.A.	1110	N.A.	23	N.A.
	50 °C - 5 km	939	873	281	191	10	3.5
	150 °C - 5 km	759	735	98	55	8	0.5
Cu/ZSM-5	25 °C - cold start	1904	1700	180	247	7	4
	50 °C - 5 km	1210	1150	53	52	9	0.7
	150 °C - 5 km	1210	1170	58	39	4	0.7

N.A. = not available.
[a] Values expressed in μmol/gcat.
[b] Calculated by Temperature Programmed Desorption in the T range : T_{ads} – 600 °C.

interferences on the analyzers), blank tests were carried out by using both mixture compositions in adsorption mode over an empty reactor, and the amounts for each pollutant were then subtracted to those calculated by catalytic tests. To confirm data reproducibility, three independent runs were carried out on selected samples, giving a confidence interval of ± 98% over concentrations reported for the main pollutants under study (HCs, NH_3, NO).

3. Results and discussions

3.1. General interpretation of breakthrough curves upon cold-start test

Breakthrough curves obtained with time on stream over all materials (NH_4/Beta, Cu/ZSM-5, Fe/Beta, Cu/Beta, Activated Carbon (AC)), under constant adsorption conditions – "cold start" and $T_{25\,°C}$ - are reported in Fig. 1. The saturation level was considered to be when the asymptotic stable concentration approached the initial value in the feed gas (see Table 2).

CO and CO_2 saturation levels (2800 ppm and 10 vol%, respectively) were attained promptly, shortly after gas injection start (at 120 s) for all the materials (Figs. 1a and 1b). For NO (Fig. 1c), almost all materials show no trapping efficiency, except for Cu/Beta, Fe/Beta, and Cu/ZSM-5 zeolites for which breakthrough reached an over-saturation before stabilizing at saturation levels. For N_2O (Fig. 1d), all the materials exhibit the same profile, with limited (but not correctly quantifiable) adsorption of a few ppm. Adsorption of NH_3 (Fig. 1e) depends on the physical-chemical properties of each material, which impose a net difference in both breakthrough times and trends. For some sorbents, the concentration increases promptly after a NH_3 short break (AC, and NH_4/Beta), whereas for all the others, the concentration increases slowly up to saturation levels with different slopes. Fe/Beta presents a specific intermediate behavior, with a long breakthrough time, but a slope similar to that of the first group.

Finally, sorption trends are reversed in cases of HC breakthrough (Figs. 1f and SI-2, at longer time on stream). For zeolites, the feedgas hydrocarbons show a zero value and then a progressive increase, complementary to the decrease in available adsorption sites, among which Fe/Beta, NH_4/Beta followed by Cu/ZSM-5 and Cu/Beta exhibit lower performance than AC. They then reach their saturation plateau (1615 ppmC, stated in terms of equivalent CH_4) content rapidly, indicating that HCs easily diffuse within the zeolite pore system without retention.

Both AC and Cu/Beta display a longer breakthrough, with two steps before reaching saturation level. Focusing on the very first seconds of adsorption, Fe, NH_4 and Cu/Beta zeolites show cyclic adsorption/desorption phenomena (presence of noisy peaks which persist along saturation time), thus indicating that a part of the amount adsorbed is desorbed before saturation owing to a displacement of the adsorption equilibrium, probably due to competitive adsorption among HCs, and/or with H_2O (Fig. SI-2). This latter aspect will be further investigated in the following paragraphs.

In summary, AC, Cu/Beta, and Cu/ZSM-5 have shown the highest trap performance in terms of number, retention time and amount of pollutants. For these, a detailed study was carried out to better understand their behavior in the additional operating conditions.

3.2. Quantitative comparison of adsorption capacity and releases

The quantitative uptakes and releases, for AC, Cu/Beta, and Cu/ZSM-5 are compared in Table 3. In general, uptakes of each sorbate are calculated from the start of injection up to reaching the plateau of saturation, whereas their releases are quantified in the interval ranging from the switch in N_2 under isotherm to the end of temperature programmed desorption (TPD). The maximum amount of sorbate that can be adsorbed per gram catalyst is referred to as the adsorption capacity. In the table, values are reported in $\mu mol/g_{cat}$ rather than in mg/g_{cat}, because the presence of multiples HCs with different molecular masses may result in misestimation. It should be anticipated that some of the calculated capacities reported in adsorption and desorption do not match within experimental error. The gap between the two amounts can be due to multiple factors, such as irreversible adsorption, catalytic conversion, or because the quantification of adsorption capacity takes into account also the fluctuations (as shown in Fig. 1). Except in a few cases, which will be debated later, the gap is negligible for all the sorbates in each sorbent, so we will focus on the results of adsorption capacity.

Adsorption capacity towards NH_3 represents from 57% to 87% of overall capacity in Cu/Beta, as T_{ads} increases. At $T_{25\,°C}$ and "cold start", the capacity is around 1500 μmol/gcat, but tends to decrease as a function of NH_3 concentration (from "cold start" to "5 km") and T_{ads} (939 and 759 μmol/gcat, at "5 km" and $T_{50\,°C}$ or $T_{150\,°C}$, respectively).

Analogously, the adsorption capacity towards HCs is the same of order of magnitude at $T_{25\,°C}$ and "cold start" (1110 μmol/gcat, ca 42% of overall capacity), and it dramatically drops at "5 km" to 281 and 98 μmol/gcat for $T_{50\,°C}$ or $T_{150\,°C}$, respectively. Under any conditions, it is worth noting only a partial release.

Finally, a poor but not negligible activity is recorded in the adsorption capacity of NO, whose desorption was one order of magnitude lower.

AC displays a moderate adsorption capacity towards NH_3 at $T_{25\,°C}$ and "cold start" (54 μmol/gcat), which decreases by a factor of 2,5 upon "5 km", proportional to the ratio in the initial concentration in the gas mixtures. At iso-concentrations, the increase of T_{ads} does not affect the adsorption capacity. On the contrary, AC shows the highest adsorption capacity towards HCs, which represents almost 99% of its overall capacity, and particularly at $T_{25\,°C}$ and "cold start" (6461 μmol/gcat). Nevertheless, its results are strongly impacted by both initial feed composition ("cold start" or " 5 km") and T_{ads} (from 2683 to 426 μmol/gcat at "5 km" and $T_{50\,°C}$ and $T_{150\,°C}$, respectively).

The highest adsorption capacity towards NH_3 among all the sorbents under study is recorded for Cu/ZSM-5 (91–95% of overall capacity), with dependence only on initial concentration in the feed but not on T_{ads}. Its poorest adsorption capacity towards HCs would suggest that this material was a bad candidate for trapping organic compounds, however this is not the case as it will be further described.

In summary, many effects emerge such as i) the T_{ads}, that unfavors adsorption as it rises, ii) the different nature of sorbent/sorbate interaction, that leads to almost reversible interactions over all the samples, iii) the lower NO adsorption capacity for Cu/ZSM-5 in respect to Cu/Beta, despite the latter having the same Cu loading, Si/Al, and similar surface area, and iv) hydrophilicity/hydrophobicity and porosity of substrates, which act in strict connection and will be further discussed.

Table 4
Comparison at the same mixture conditions of quantitative uptake (ads) and release (des) of AC, for each T_{ads}.

Sample	T_{ads}	NH_3[a]		HCs[a]		NO_x[a]	
	°C	*ads*	*des*[b]	*ads*	*des*[b]	*ads*	*des*[b]
AC	25	54	55	6461	5778	11	7.4
Cold start mixture	50	43	51	4430	4700	22	3
	150	44	43	1190	1170	23	2
AC							
5 km mixture	25	NA	NA	NA	NA	NA	NA
	50	23	14	2683	3107	6	5.5
	150	21	23	426	445	6	0.5

N.A. = not available.
[a] Values expressed in μmol/gcat.
[b] Calculated by Temperature Programmed Desorption in the T range: T_{ads} – 600 °C.

From this comparison, it is also evident that none of the sorbents under study is efficient towards all the pollutants simultaneously, with the AC and Cu/ZSM-5 showing preferential performance towards HCs and NH_3 respectively, and Cu/Beta an intermediate efficiency for all.

3.3. Quantitative comparison of uptakes and releases at iso-conditions

Previous results highlight that the combination of exhaust gas concentration and T_{ads} have a great impact on competitive adsorption of the pollutants. In order to discriminate each contribution, a systematic comparison of adsorption capacities has been carried out by using a "cold start" or "5 km" mixture at all the T_{ads}. Data are reported in Table 4 for AC. The missing values for $T_{25\,°C}$ and "5 km" are imputed to the high content of water in the stream which leads to condensation on the cold parts at 25 °C, and thus a significant interference. As a confirmation, when the "cold start" is used (more concentrated mixture), NH_3 capacities are not affected. An overall higher adsorption capacities of HCs is recorded, although unfavored at increasing T_{ads}, and NO. These findings confirm the major role of the partial pressure.

3.4. HCs speciation

3.4.1. HCs-TPD and speciation over AC

The qualitative and quantitative speciation of each HC along the adsorption and release has been followed by on-line analysis by μGC [15] for AC, at "cold start" at $T_{25\,°C}$ (Fig. 2a), and "5 km" at $T_{50\,°C}$ (Fig. 2b) and $T_{150\,°C}$ (Fig. 2c), respectively.

Despite the correspondence shown in Table 3, the measure of pollutants having small concentrations, or those to have undergone to side reactions, can be affected by an error. However, even with uncertainties in measurement, a qualitative trend may provide useful insight, and will be explored in a further investigation during a second phase over corresponding monoliths (not shown here).

For AC at all T_{ads}, only the adsorption of n-pentane, i-pentane and toluene occurs, whereas for methane, acetylene, and ethylene, the sorbent shows no adsorption capacity.

In view of the reversible adsorption/desorption behavior, we followed the speciation also during TPD runs (by rising temperature at saturation condition), to get insights about the nature of sites implied in the adsorption process. This has also been employed to implement a modeling system which helps to predict the best configuration for a zero emission control in real systems [14]. HCs-TPD curves and their corresponding deconvolutions are depicted in Fig. 2 (from a′ to c′). To find a model method, the same deconvolution protocol has been adopted for all the curves under study and readapted in order to match literature data (if available) with experimental evidence. Indeed, species involved in each desorption peak were identified by cross-matching measurements of total HCs by FID with those by μGC. Assuming a Langmuir kinetic formalism for storage trend and a Temkin-type reaction rate expression for desorption of each site, deconvolution was realized over TPD run after $T_{150\,°C}$-"5 km" test and determining the parameters values to best fit the experimental datas. Then, the same deconvolution was applied for the tests $T_{50\,°C}$-"5 km" and $T_{25\,°C}$-"cold start" and, when needed, an incremental number of storage sites were added at different Temperature maxima, until the deconvolution was consistent.

For AC samples, a broad signal is observed with multiple components underneath. The temperature maxima of deconvoluted peaks do not shift with T_{ads}, indicating that the bonds between HCs and active sites of

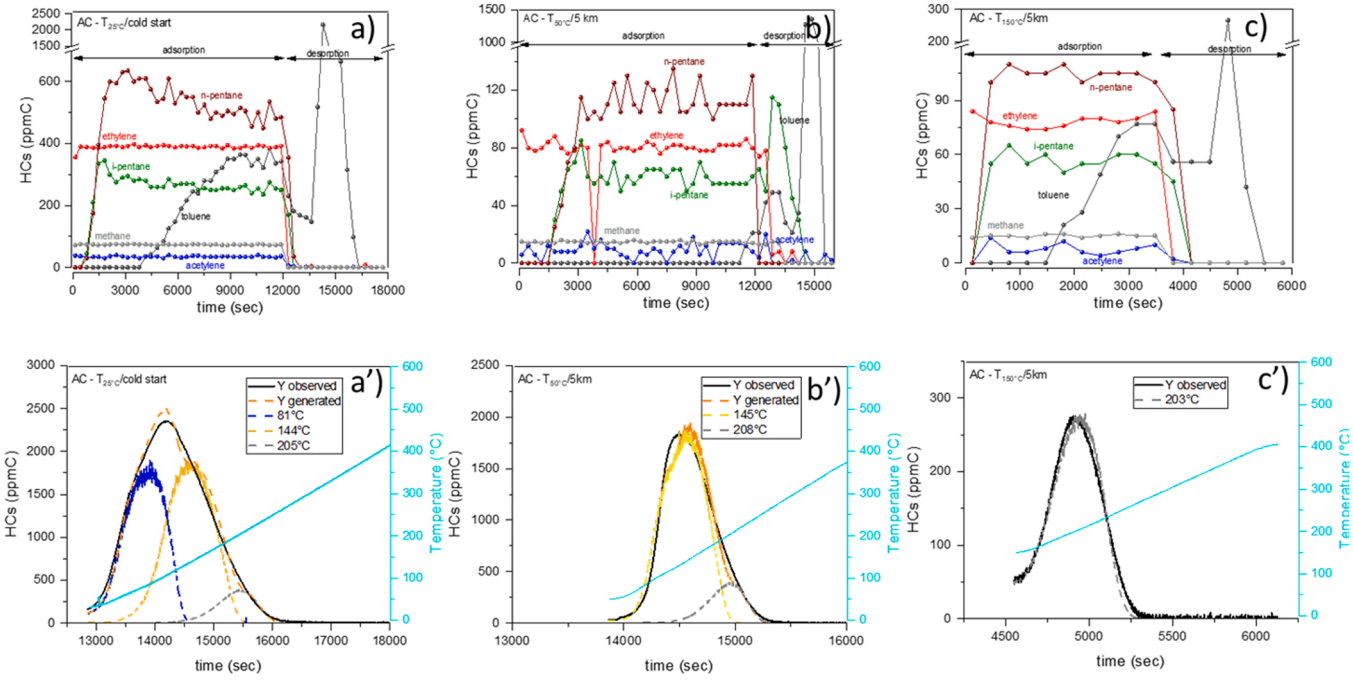

Fig. 2. a/b/c) HCs speciation via μGC runs during adsorption and TPD runs and a′/b′/c′) HCs-TPD profiles over AC at the three different T_{ads}.

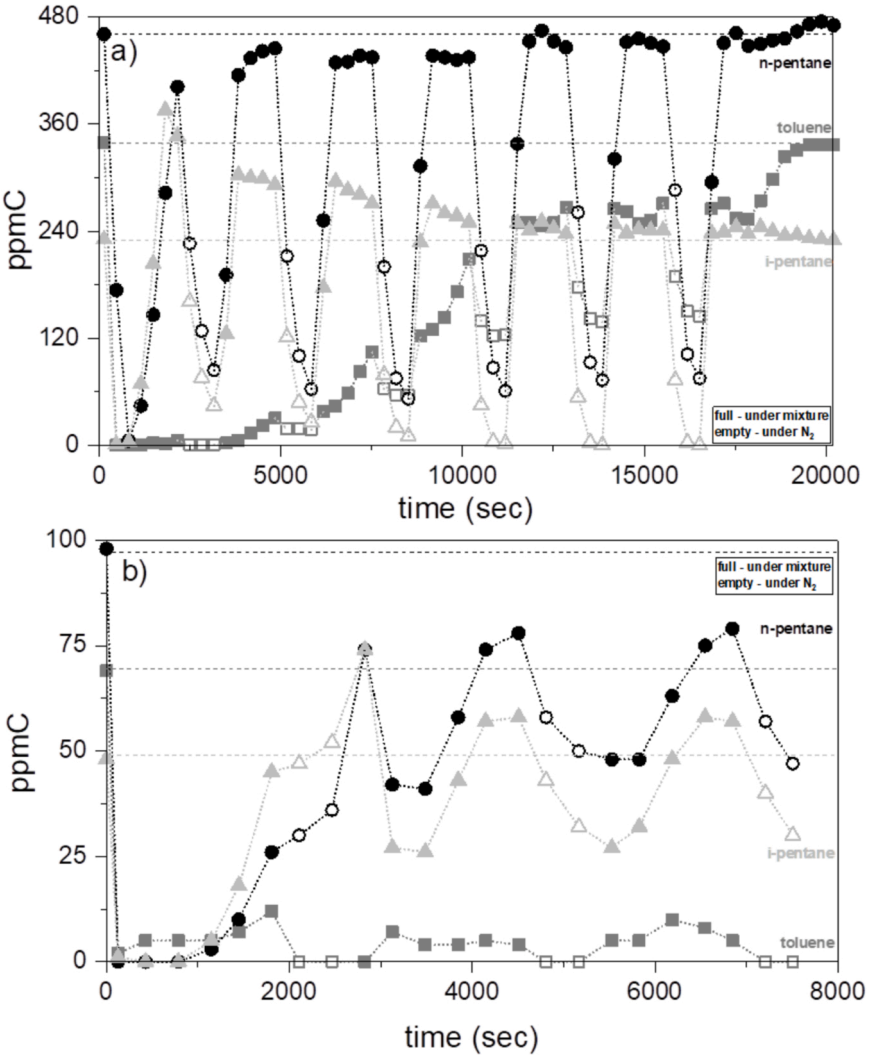

Fig. 3. Transient profile by μGC of toluene, n-pentane and i-pentane concentrations over AC using "cold start" (a) or "5 km" (b) mixtures at $T_{25\,°C}$ and $T_{50\,°C}$, respectively, using cycles of 30 min under mixture and 15 min under N_2 flows.

sorbents have the same activation energy (E_{act}). Moreover, the decrease in absolute intensity (from 2500 ppmC in $T_{25\,°C}$ to 250 ppmC for $T_{150\,°C}$), which accounts for a difference in relative abundance, reflects the differences observed in absolutes uptakes (Table 3). According to the observation that the number of peaks decrease as T_{ads} increases, some adsorptions over active sites could be unfavored at higher T_{ads}, or/and desorption may occur at the end of saturation due to the switch into N_2 before TPD run (corroborated by the non-zero baseline for $T_{150\,°C}$), induced by the change in partial pressure.

During all the TPD only toluene is quantitatively released. The overlap of TPD curves to their corresponding μGC runs, obtained over AC sample by using the same "cold start" mixture but at the three T_{ads} confirmed that toluene is the only implied (Fig. SI-3). The fact that the trends are qualitatively the same, independently from the mixture used, confirms that the different behavior observed for AC at $T_{25\,°C}$, $T_{50\,°C}$ and $T_{150\,°C}$ under any mixture condition can be imputed mostly, but not exclusively, to the T_{ads}. Whereas, the higher uptake (and release) observed when using a more concentrated mixture at the same T_{ads} accounts for the difference in partial pressures of pollutants in each feed gas.

3.4.2. *Mimicking a start and stop over AC*

Isothermal cycle experiments, using regular switches between mixture (for 30 min) and N_2 (15 min) at $T_{25\,°C}$ and $T_{50\,°C}$ over AC, have been carried out to better elucidate which is the most dynamic adsorption process, and to represent a non-steady state condition typical of a vehicle run (Fig. 3). Then, after a break overnight at room temperature under air without flow, TPD was run over samples. Except for toluene, n-pentane and i-pentane, all the other pollutants weren't adsorbed in significant amounts.

In the case of $T_{25\,°C}$ under "cold mixture" (Fig. 3a), toluene is continuously stored, increasing slowly up to its saturation level over long time (340 ppmC at 20.000 s ca), with negligible release during the periods under N_2 for the first 2 runs. From the 3rd cycle under N_2, a more important quantity starts to be released. Its different profile in the first 3 cycles using $T_{50\,°C}$ under "5 km" (Fig. 3b) allow us to confirm a dependence of toluene adsorption from its partial pressure.

N-pentane and i-pentane, instead, have a different behavior in the two experiments. At $T_{25\,°C}$ under "cold mixture", i-pentane is first adsorbed but then increases its concentration quite fast in the outlet stream reaching a value above its saturation level (230 ppmC). Then a small part is then released under N_2. Starting from the 2nd run it is irreversibly adsorbed as no i-pentane was detected under N_2, and slowly declines up to its saturation level at 20.000 s. Conversely, n-pentane adsorbs mostly with a *start and stop* behavior under "mixture" and N_2, respectively without dropping to zero under the N_2 phase. At each cycle, it adsorbs in small quantities until reaching its saturation value (460 ppmC), at around the 5th cycle. From then on, it does not uptake

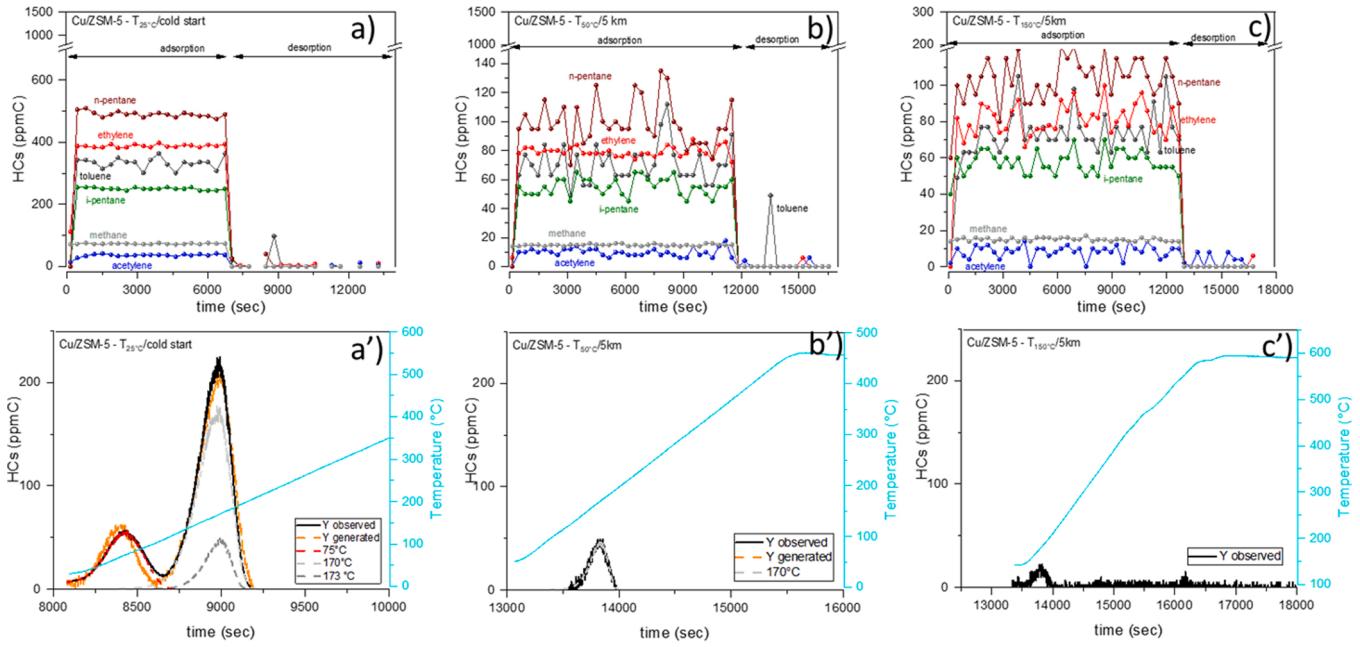

Fig. 4. a/b/c) HCs speciation via μGC runs during adsorption and TPD runs and a′/b′/c′) HCs-TPD profiles over Cu/ZSM-5 at the three different T_{ads}.

anymore, but it is released during N_2 phase in significant amounts.

I-pentane and toluene display a specular pattern, more marked at higher concentration in the $T_{25\,°C}$ under "cold mixture" experiment. Nevertheless, TPD profiles run after reaching saturation and leaving the reactor open in air overnight, reveal a quantitative release only of toluene, and, also in this case, i-pentane and n-pentane were not detected during TPD. These findings let us confirm that during experiments, i-pentane is replaced by toluene, and both i-pentane and n-pentane are desorbed before the TPD run.

Looking at the overall profile of the three HCs at the very first seconds, we may speculate that toluene, i-pentane and n-pentane are quantitatively adsorbed simultaneously over different active sites of AC without competing each other at first steps. Indeed, their concentration drops rapidly to zero soon after injection. Then, toluene does not break promptly, whereas i-pentane reaches a value which is well above its saturation level, thus suggesting that adsorption of i-pentane occurs as fast as a part is simultaneously desorbed, probably boosted by the incoming adsorption of the two others. At this stage, it is reasonable that only sites having medium-strong strength are implied in the adsorption process for toluene and small amounts of n-pentane. Whereas, most of n-pentane and i-pentane occupy weaker adsorption sites. Further, during the second switch under N_2, a small part of toluene starts to be released, leaving some "sitting sites" available, soon occupied by free pentanes. The hypothesis that the mobility of pentanes is not only a function of punctual concentration, but also of T_{ads} is corroborated by the experiments performed under "5 km" and $T_{50\,°C}$ (Fig. 3b), where i-pentane and n-pentane differ in the first run under N_2, with a remarkable desorption of both. Thus, the over-accumulation of i-pentane observed at $T_{25\,°C}$ can be imputed to a real desorption process which takes place within the pores of AC rather than an effect of diffusion along the pores of the sorbent [16].

Only after 5 runs under mixture, the concentration in the outlet stream of i-pentane and n-pentane stabilize at saturation level. While i-pentane rapidly drops under N_2, confirming that there is no further uptake by AC, n-pentane undergoes a significant desorption. The difficulty of AC to adsorb the n-pentane has been also confirmed by Moreno-Piraján et al. [17]. They proved that the n-pentane capture capacity of the parent AC would be significantly enhanced only by the thermal treatment, or AC functionalization. Toluene still undergoes to unbalanced adsorption/desorption during mixture and N_2 runs, respectively, thus suggesting that only active sites with weak to medium adsorption capacity left by both n-pentane (during isothermal desorption) and i-pentane (by replacement) are now employed only by toluene [18]. Those could be associated to the multiple peaks observed in TPD deconvolution curves (Fig. 2).

Finally, in the last run, where the gas stream was admitted for a longer time, toluene, i-pentane, and n-pentane attained stable saturation. At the end of the overall adsorption process, the quantity of n-pentane is significantly lower than that of i-pentane, indicating that over AC the adsorption of i-pentane and toluene is thermodynamically favored [19,20]. Nevertheless, during TPD, the overall amount of HCs detected by FID matches with that of toluene quantified by μGC; moreover, no C_5 peaks are detectable by μGC but some parasite peaks appear, which may suggest the occurrence of secondary reactions favored by rising temperature during TPD.

3.4.3. *HCs-TPD and speciation over Cu/ZSM-5*

Fig. 4 depicts the HCs adsorption and release trends over Cu/ZSM-5 zeolite. At all $T_{ads,}$ lower adsorption is observed over Cu/ZSM-5 zeolite than over AC. This reflects the lower adsorption capacity of Cu/ZSM-5 zeolite listed in Table 2. In particular, at $T_{50\,°C}$ and $T_{150\,°C}$ the signals are very noisy with important fluctuations (± 50 ppmC, except for methane), likely due to easier uptake/release movement of NMHCs inside the ZSM-5 channel during the temperature test. At $T_{25\,°C}$, only two distinct zones are present (with temperature maxima centered at 75 °C, 170 °C and 173 °C, respectively), while at $T_{50\,°C}$ only a component centered at 170 °C is present. Finally, the TPD performed after $T_{150\,°C}$ presents a low, noisy signal which makes impossible to deconvolute.The affinity of ethylene to the MFI framework is well known [21] when it is not in competition with other molecules. Upon co-feeding, water and ethylene can compete over Brønsted acid sites (*B)* but, owing to less basic character of the latter and its minor concentration in the stream, it is reported that water adsorption always prevails. In the $T_{25\,°C}$ and " cold mixture " run over Cu/ZSM-5 (Fig. 3), we observed a controversial behavior, that may accounts for the formation of some species responsible for the desorption peak at 75 °C in the corresponding TPD run.

Indeed, the adsorption capacities differ significantly when using only a simple HC mixture (Fig. SI-4) under dry conditions. In this case, we did not observe any ethylene or acetylene adsorption, but only toluene, n-pentane and i-pentane (Fig. SI-4d). Accordingly, this is an indication

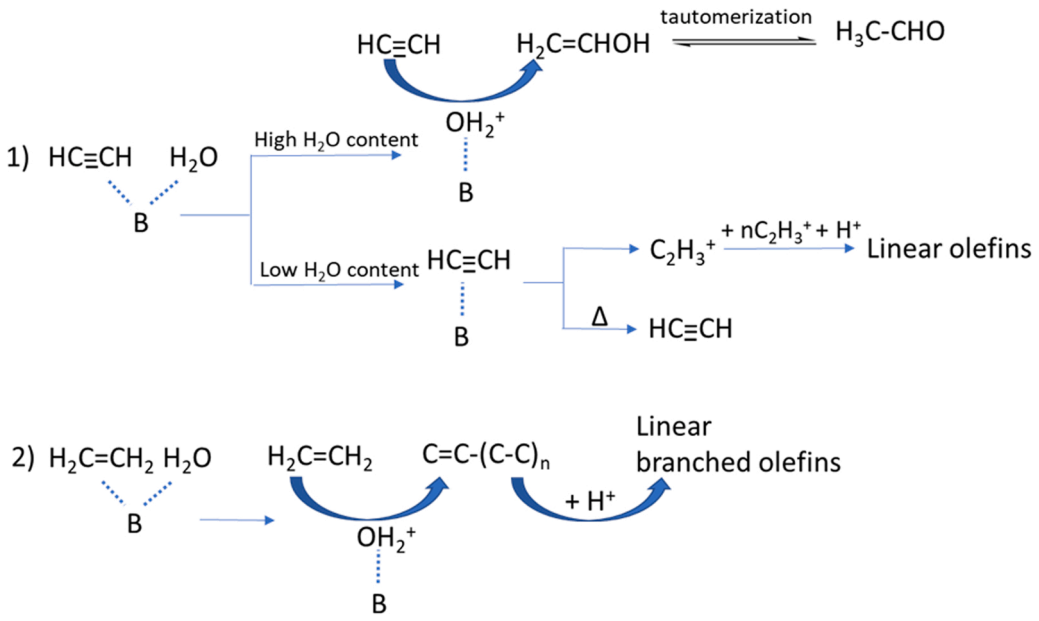

Scheme 2. Schematic representation of possible reaction pathways for 1) acetylene and 2) ethylene upon adsorption over Brønsted sites.

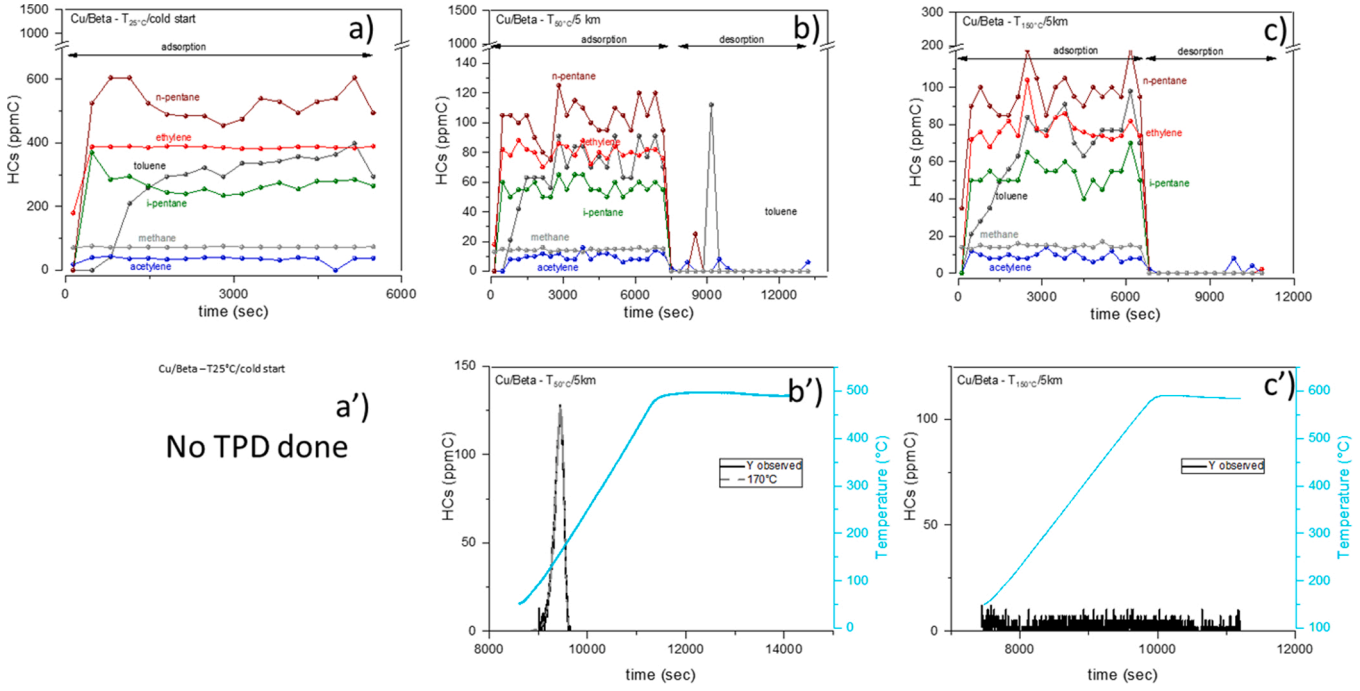

Fig. 5. a/b/c) HCs speciation via μGC runs during adsorption and TPD runs and a′/b′/c′) HCs-TPD profiles over Cu/Beta at the three different T_{ads}.

that under wet conditions a further bonding of ethylene occurs with *B*-OH_2^+ adduct (formed by preferential adsorption of water at initial stages). As it is known, once the surface gets alkylated a slow oligomerization initiates even at room temperature leading to a broad distribution of paraffinic carbon atoms [22]. Finally, for all the three T_{ads}, during TPD in Cu/ZSM-5, only traces of toluene, acetylene and ethylene are evidenced. Being that these latter concentrations are at the limit of their detection levels, this may indicate that the adsorbed acetylene and ethylene are indeed converted. At increasing T_{ads} the residence time of H_2O on the site within the pores becomes shorter and, as water promotes the ethylene adsorption and consecutive reaction, as a consequence also that of reactive HCs.

Adsorption of acetylene and water on Cu/based zeolites resulting in hydration to acetaldehyde has been previously reported by [23] even at 25 °C. The authors convey that (1) both water and acetylene adsorb on the same kind of site; (2) at higher H_2O coverages, acetylene reacts with it, and acetaldehyde is formed; (3) at low H_2O coverages, adsorbed acetylene may react with another acetylene molecule or kept adsorbed as such. A schematic representation of the possible pathways for both ethylene and acetylene is reported in Scheme 2.

These findings are in line with our observation, since at TPD after adsorption at $T_{150\ °C}$ (so low water coverage), a weak signal of acetylene appears amounts. As a confirmation, by use of Cu/ZSM-5 monoliths (not shown here), where powder loading is much higher, extra peaks in FID signal during TPD do not have quantitative correspondence with the followed hydrocarbons in μGC runs.

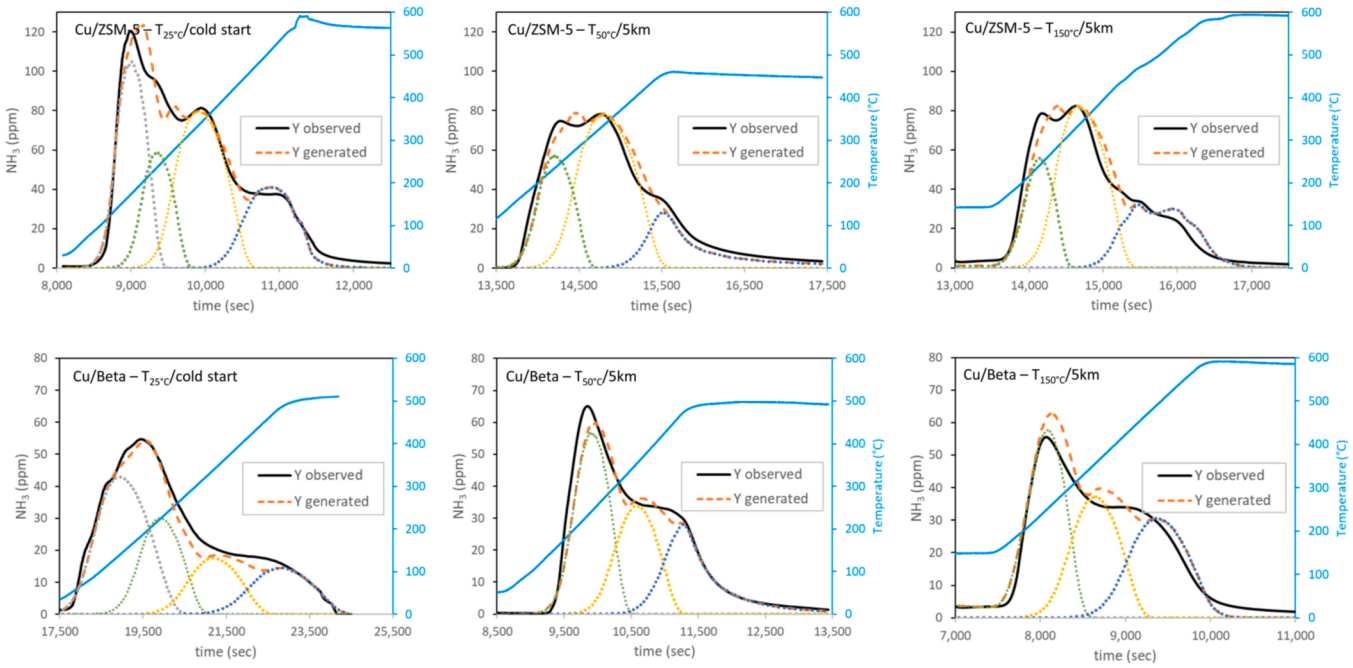

Fig. 6. NH_3-TPD profiles over Cu/ZSM-5 and Cu/Beta at the three different T_{ads}.

3.4.4. *HCs-TPD and speciation over Cu/Beta*

In case of μGC runs over Cu/Beta at $T_{50\,°C}$ (Fig. 5), analysis results are very noisy, also for more abundant pollutants, with fluctuations of ± 10 ppmC in some cases. This would suggest that dynamic adsorption/desorption phenomena take place, boosted probably by the presence of H_2O (as explained later, see Fig. SI-5). Higher amounts of ethylene, toluene and acetylene are adsorbed in the first seconds, but during TPD only traces of acetylene, ethylene, n-pentane, and small amount of toluene appear at $T_{50\,°C}$. None of these features are remarkably observed in the TPD run after $T_{150\,°C}$.

In comparison with the Cu/Beta at the same T_{ads}, the asymmetric TPD profile over Cu/ZSM-5 at $T_{50\,°C}$ hinders a main component at 170 °C and others less intensely at lower temperatures. This lets us think that the two zeolites do not use the active sites in the same way, due probably to many factors such as i) an impact of the different diffusivity in the 3D zeolites on the interaction between the same HC and different neighboring active sites, ii) the same active site interacts trough the same functionalities present in the different HCs of the mixture or iii) during adsorption, some side reactions occur which may lead to the formation of other HCs interacting with the same active sites via multiple bondings. The absence of a net signal for TPD run at $T_{150\,°C}$ may indirectly indicate that some of these effects may coexist and are amplified in a way to give back a scattered signal.

In general, the results indicate that i) AC displays a better adsorption capacity towards heavy NMHCs, such as toluene and pentanes (but under desorption only toluene is observed), and ii) Cu/ZSM-5 and Cu/Beta adsorb preferentially light NMHCs (ethylene, acetylene) and a small amount of toluene (but under desorption only this latter is released).

3.5. *NH_3-TPD over Cu-based zeolites*

Similarly to the method used for HCs-TPD deconvolution, NH_3-TPD profiles were explored for those sorbents that showed up a net signal, notably Cu/Beta, and Cu/ZSM-5 (Fig. 6). As the NH_3 storage ability has been widely studied, storage sites characteristics can be found in the literature to adapt and deconvolute TPD signals.

For both Cu/ZSM-5 and Cu/Beta, three distinct features centered at 230 °C, 350 °C, and 470 °C are always present in the higher T_{ads} and

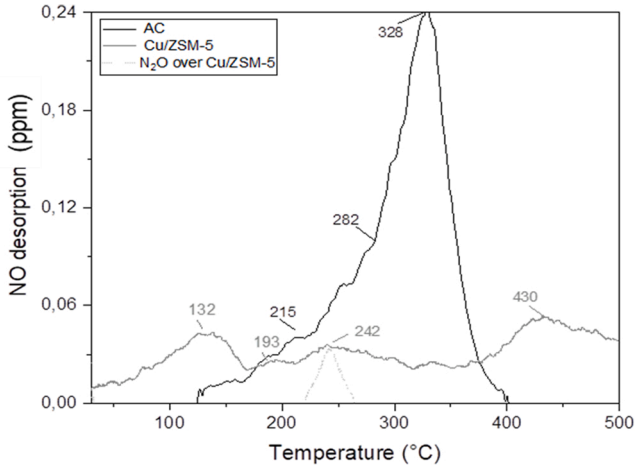

Fig. 7. NO-TPD over AC and Cu/ZSM-5 and N_2O-TPD for Cu/ZSM-5 sorbents at "cold start" mixture and $T_{25\,°C}$.

"5 km" mixtures, whereas another peak can be envisaged in both for the $T_{25\,°C}$ and "cold start" runs centered at 150 °C. In most cases there are several NH_3 desorption peaks, and thus binding strengths [24]; during TPD, an acid site only releases ammonia when all of the less strongly bound NH_3 has been released. At high concentration of strong acid sites, this result is much more hindered in the zeolitic channels. When the Brønsted sites release NH_3 in form of NH_4^+ ions, these latters have a Lewis acid character which, if no stronger acid is available, can also re-adsorb NH_3. The desorption of NH_3 on the NH_4^+ ions is attributed to the higher temperature component. According to these findings, TPD peak appearing at about 150 °C and 230 °C can be associated to physical or weak chemical adsorption, whereas the desorption maximum observed usually above 300 °C can belong to NH_4^+ (weak Lewis acid) decomposition into $NH_3 + H^+$ (strong Brønsted acid hydroxyl groups) [25]. Zhang et al. [26] found that the NH_3-TPD spectra of Cu zeolites consisted of three distinctive desorption peaks centered at ~ 170, ~ 240, and ~ 340 °C. which are attributed to the weak (α), moderate (β), and strong (γ) acid sites, respectively. The moderate acid sites were

attributed by the substitution of surface protons by copper ions and thus are assigned to ammonia adsorbed upon copper ions on Cu-ZSM-5 catalysts. In the Cu-exchanged zeolites, the bands of Brønsted bound NH_3 probably developed from the interaction with protons generated during the dehydration by the heterolitic dissociation of water coordinated to the Cu^{2+} cations. In our sample, both the samples display the same kind of sites, but the relative abundance change in respect to the T_{ads} and not the partial pressure.

3.6. NO-TPD over AC and Cu-based zeolites

Literature reports that AC and zeolites are very prompt to adsorb NO molecules [27], but in our test conditions we observed a detectable weak release upon TPD only over AC and Cu/ZSM-5 under $T_{25\,°C}$ and "cold mixture", as reported in Fig. 7. For AC, NO was released at high temperature, with the presence of three peaks centered at 215, 282 and 328 °C, respectively. They correspond to the weakly adsorbed NO and strongly adsorbed NO, mainly in the form of $(NO)_2$ dimer [28]. The shift at higher temperatures than usually reported in literature, and the number of peaks let us suggest that other pollutants present in the feed are responsible for the strongly adsorbed NO. But due to the low signal level, it is difficult to give a clear assignment of which pollutant can be responsible for that. Zhu and coworkers reported that the oxidation of NO in the gas phase was very slow at low temperatures and low NO and O_2 concentrations [29]. This finding suggested that NO oxidation in the gas phase may only have a minor role for the NO adsorption.

Despite of the low signal, several NO desorption peaks can be detected over Cu/ZSM-5, centered at 132, 193, 242 and 430 °C respectively. These T maxima are slightly higher than those reported in literature [30] accounting for an higher binding energy of NO. It is also reported that NO disproportionates to N_2O and NO_2 at 25 °C, and the N_2O formed decomposes further to N_2 and O. Thus, this highlights the importance of monitoring N_2O simultaneously. In our case, we didn't observe any NO_2 signal nor an increase in N_2O amount during adsorption phase in the outlet stream, but rather a very small release of N_2O at high temperature (242 °C), close to detection limit. Nevertheless, since we observed the disproportion reaction over Cu/ZSM-5 monolith (extra tests not detailed here), we can conclude that in such lower amount of catalyst the side products are produced in amount below detection limits.

Differently for NH_3, we didn't observe any dependence to H_2O (Fig. SI-5) but the optimal NO_x desorption temperature may vary from case to case. However, for an exhaust ATS consisting of an NH_3-SCR unit, NO_x release should at least start no lower than 200 °C. NOx trap materials have to operate under appropriate conditions, i.e. when the gas phase temperature increases rapidly. In these conditions, NOx uptake at a low temperature (typically less than 100 °C) would be preferred, to minimize the amount of the catalyst that is required for cold start NO_x storage. To ensure the maximum utilization of the storage capacity, NO_x adsorption and cold start duration need to be at least on the same time scale. Nevertheless, as NO oxidation to NO_2 (fundamental to operate for LNT) is kinetically limited, NO diffusion within the porous system of sorbent as well as the adsorption on the storage sites have to be as fast and quantitative as possible [30], to allow the ATS (LNT, for instance) to work properly. In this context, AC is a cost-effective solution for NO_x removal. The adsorption capacity could be improved by surface functionalization [31]. Currently, NOx traps typically contain Platinum-Group Metals (PGM) [32], so the choice of a cheaper metal has been evaluated here, to provide a multipollutant removal strategy without internal competition, and resistant to poisoning [9]. Nevertheless, an excessive desorption temperature will render it more difficult to regenerate the catalyst, as requiring higher desorption temperature could result in incomplete desorption and therefore less effective storage for the next cold start cycle. When evaluating catalyst performance, this degradation can be reflected by a decrease in low temperature NOx storage capacity, and/or a shift in desorption temperature into a non-optimal range. Addition of Fe to the inlet zone of a Cu/zeolite catalyst also helps to mitigate N_2O formation. There is a trade-off: N_2O was reduced with addition of Fe up to 20% of the inlet zone beyond which there is little/no further reduction, along with a loss in NO_x conversion. In our tests, we observed a lower performance in NO adsorption for all the materials during study, thus suggesting that under real conditions, this molecule is not the favorite, as it would be when injected alone [33] or co-fed with fewer compounds [34,35].

4. Discussions

4.1. NAQIV approach

The objective of this study is to develop a Neutral Air Quality Impact Vehicle (NAQIV) using a system able to reduce the tailpipe emissions of a gasoline powertrain engine. Although the criteria to assess local air quality can vary as a function of engine, fuel and country, similar results in zero emission control have to be expected. Regulations and auto makers plan a long-term increased of vehicle electrification, to reduce local pollutant emissions, such as pure battery electric vehicles (BEV), hydrogen fuel cell vehicles (FCV) or plug-in hybrid electric vehicles (PHEV). All these solutions are considered as zero-emission vehicle (ZEV). With continued improvement in air quality following vehicle emission reductions, data and observations indicate that also ICE (internal combustion engine) vehicle emissions may be approaching a ZEV-equivalent level [36]. In our approach, we have chosen the strategy to use cold trap sorbent after a ICE. Accordingly, the emissions considered in this work are thus related to the local pollutants, not the Green House Gases. The focus is on exhaust vehicle emissions although the non-exhaust emissions have to be taken into account (their analysis have not been included in this paper). The target is to reach low tailpipe emissions determined by air quality simulation, in order to have a neutral impact of the vehicle on air quality in urban areas. The proposed neutrality is obtained by simulating a fleet of NAQIV, by modeling the emission–immission interaction as reported by Steinhaus [37] in urban areas.The authors showed that both background and street pollutant levels are constant or show a low increase not exceeding 10–15%. They also reported the impact of NOx tailpipe levels on the air quality at the street level using such modeling. A low level of NOx close or below 10 mg/km allows to reach close to neutral air quality impact. Among the local pollutants identified, the data reported in this study shows that NO, NH_3, traces of N_2O, H_2O and NMHCs are the only species involved in adsorption processes under the adopted conditions. For the rest of pollutants (CO, CO_2, CH_4), none of the sorbents display any adsorption capacity. For the first time, it is here showed that under representative driving conditions, the competition in adsorption can be reduced to the evaluation of binary interferences, where the common denominator is H_2O. Massive adsorptions of NH_3 and very small N_2O are observed on Cu/zeolites, while NMHCs and few NO prevalently over AC, although this sorbent seems to be a good trade-off for an average adsorption of almost pollutants in the feed.

4.2. Unraveling the effect of water on HCs adsorption

In our study, HCs adsorption capacity tests were performed by use of a 'simple' mixture of 6 HCs (toluene, methane, ethylene, acetylene, i-pentane and n-pentane), focusing on those most present in an exhaust gas of a vehicle driven under real conditions. Whilst other HCs could be also conceivable, these 6 HCs represent the model molecules (alkanes, alkenes, alkynes, isomers and aromatics) heading to heavier and more complex compounds that can be generated by secondary reactions (cracking, isomerization, polymerization, alkylation for instance), catalyzed by temperature and active sites of the ATS [38]. Nevertheless, the total amount of HCs that can be adsorbed over the sorbent is limited, and therefore it is important to model the adsorption behavior onto the sorbent. For this purpose, we described how the sorption properties

decrease during the sorbent lifetime, as well as the sorbate-sorbent interaction through transient and TPD runs, respectively. An aspect which is often neglected is the distinction between overall mass trap efficiency and adsorption capacity.

As example, in our mixture toluene, n-pentane and i-pentane represent not only the heavy NMHCs in terms of molecular mass, but also the most abundant in the HCs feed. Since our mixture is composed by 68% of heavy HCs (in terms of cumulative ppmC in toluene, i-pentane and n-pentane) and 32% of light HCs (in terms of cumulative ppmC of ethylene, acetylene, methane), the adsorption capacity should be evaluated according to speciation, as evidenced by following the profile of μGC runs. This may give an overall negative or positive HCs adsorption capacity, caused by a decrease or increase in the mass efficiency. The mass trap efficiency is closely related to the distribution of hydrocarbon species in the exhaust; to the extent that adsorption of small molecules predominate (as for Cu-zeolites), the adsorption capacity results negligible, but the mass trap efficiency is definitively high. Whereas, if we look at results over AC, we reach almost 100% mass trap efficiency for toluene, with slight contribution of i-pentane and n-pentane, but in terms of adsorption capacity we reached around only 22% of the global NMHCs mixture. Moreover, we have shown that small variations of temperature (in respect to what potentially observed in a vehicle), as well as time on stream play a key-role. Indeed, the overall study highlights that each sorbent presents pros and cons in respect to the utilization. The choice of a proper architecture of an "ideal" sorbent should take into account all these factors.

AC, in respect to its lower cost, can be suitable for a wider range of VOCs. But its adsorption capacity would remarkably decrease in presence of more volatile compounds, and along time on stream (at expenses of heavy HCs). Whereas zeolites, which demand a higher initial investment, are good candidates for high polar molecules, as NH_3, N_2O, and lighter VOCs.

Considering the latter aspects, it has to be recalled that diffusion in the micropores of a zeolite is usually described as “configurational” and has been assimilated as surface diffusion because of the small distance between the molecules and the pore wall. The diffusivity in this regime has been reported to be much more temperature-dependent than gas-phase diffusion. It depends strongly on the sorbate concentration, pore diameter and structure of the sorbent, the interactions between the surface atoms and the diffusing molecules, the shape of the diffusing molecules, and the way the channels are connected [39,40]. BEA zeolites present high accessibility, making it possible for bulky molecules to interact with all the acidic centers present in the catalyst. Burk et al. reported that BEA zeolite is a promising material to trap both propene and toluene. On the other hand, the acidity properties of zeolites influence the HCs adsorption efficiency due to their selective interaction of each acid site (Brønsted or Lewis). We observed a similar behavior under dry conditions, i.e. injecting only the pure 6 HCs onto the sorbents (Fig. SI-4b and 4d), but when they are co-fed in the complex “cold start” mixture, the total ppmC adsorption profile (Figs. 4 and 5) becomes steeper, and μGC speciation significantly change, with evident adsorption of ethylene and acetylene within the very first seconds. In literature, it is reported that in almost all the commercial sorbents the adsorption of aromatics and/or heavy (long-chained) hydrocarbons ($\geq C_5$) is promoted at the expense of the light hydrocarbons, with a moderate adsorption capacity of C_4, and almost inertness for C_1–C_3 [41,42].

In conclusion of our experiments, we can state that this cannot be generalized.

Even in complex conditions as we tested, the sorption of heavy NMHCs is rather governed by the hydrophobicity of the sorbent or absence of water, such as for AC and dried zeolites. Indeed, in dry and wet conditions, AC shows similar both mass trap efficiency and adsorption capacity. For hydrophilic sorbents, such as Cu-zeolites, the presence of H_2O in the feed plays a crucial role. Adsorption capacity of light NMHCs takes advantage of prior H_2O adsorption [40], which might favor a multistep adsorption and conversion over acidic sites. This is an outstanding result, as the adsorption of light NMHCs has been always reported challenging, because of their weak interaction with zeolites, their easy release before ATS becomes operative, and the negative impact of H_2O on their adsorption [42]. In presence or absence of H_2O, for both Cu/Beta and Cu/ZSM-5, the mass trap efficiency differs significantly from adsorption capacity.

The NMHCs removal is of crucial importance for a better performing ATS, such as a NH_3/SCR [42]. For example, Nam et al. [43] clearly demonstrated a general trend in the HCs adsorption and deNOx activity: the HCs adsorption capacity of the Cu zeolites is closely related their poisoning, leading to decreased activity of Cu zeolite catalysts in NH_3/SCR.

4.3. *Effect of NH_3 solubilization on adsorption capacity*

Cu/ZSM-5, and Cu /Beta have the highest adsorption capacity of NH_3. According to literature, it seems that the modification of zeolite can improve the N-based molecules adsorption efficiency (including also NO_x). Indeed, the introduction of Cu into zeolite can facilitate the formation of moderate acid sites as well [26]. Farrusseng reported that the sorbents impregnated with reactive Cu^{2+} species (Cu/Beta, Cu/ZSM-5) have proved to offer a high ammonia fixation to yield complexes or basic-acid adducts in a ratio close to 1:1. [44]. The authors stated that the high dipolar moment of NH_3 is one of the main reasons for selectivity of zeolite toward NH_3, and removal of H_2O molecules from the zeolites framework by increasing the temperature can facilitate the NH_3 sorption processes. Then, as the T_{ads} rises from ambient temperature to 50 °C and 150 °C, breakthrough point should only be reached after longer time and consequently the adsorption capacity should increase. Surprisingly, we found an opposite trend, with unfavored NH_3 uptake at rising T_{ads}. The regime which governs the uptake, i.e. chemical or mass transport, can explain the steep profiles for AC, where there is obviously no mass transport limitation, which instead may occur in Cu/ZSM-5 and Cu/Beta. As we can exclude any impact of different packing or grain size, since all samples were sieved within a narrow size range of 200–350 μm, ammonia uptake must depend on the amount of water that is condensed at low T_{ads}, suggesting a solubilization-like mechanism. The solubility of NH_3 in water is indeed a function of NH_3 pressure, assuming undissociation of NH_3, according to Henry’s law. Farrusseng at al. have also proved that ammonia uptake mainly follow the Henry law suggesting a solubilization-like mechanism which occurs when water condenses in the pore, whilst the effect of surface interactions (i.e. confinement) might be purely responsible for the higher uptake. We may add, from our results, that the equilibrium among the solubilization, physisorption and chemisorption processes only depends on T_{ads}. The "carrier" role of H_2O is confirmed by our TPD results, where we observe the same amounts of peaks at the same E_{act}, but differing in relative abundances for all $T_{ads.}$ The fact that the absolute NH_3 uptake decreases with $T_{ads,}$ seems rather to confirm that temperature has a negative impact over H_2O adsorbed (as would expected) and, as a consequence, of the NH_3 solubilized in it. Another evidence is the simultaneous fluctuation of H_2O and NH_3 signals along saturation time (not observed in the other pollutants, for example), more marked in zeolites rather than AC.

In case of Cu/ZSM-5 it is reported that a strong interaction with the sorption sites poses energetic hindrance to the intracrystalline transport of the molecules at low coverages. At higher pressures, the high-energy sorption sites are saturated by the sorbate and the interaction of the sorptive with the sites already holding sorbate and the sites left uncovered is much weaker. Transport within the pores is facilitated, thus inhibiting adsorption from gas phase [45].

We can thus conclude that H_2O has a beneficial effect on NH_3 adsorption, at lower $T_{ads.}$ As confirmed, few ammonia adsorption (and desorption) was detected in AC when water was co-fed. In case of NH_3 adsorption onto AC powder, Rodrigues et al. [46] showed that an increase in temperature led to a decrease in adsorption capacity. This pattern is related to the type of adsorption involved in these experiments

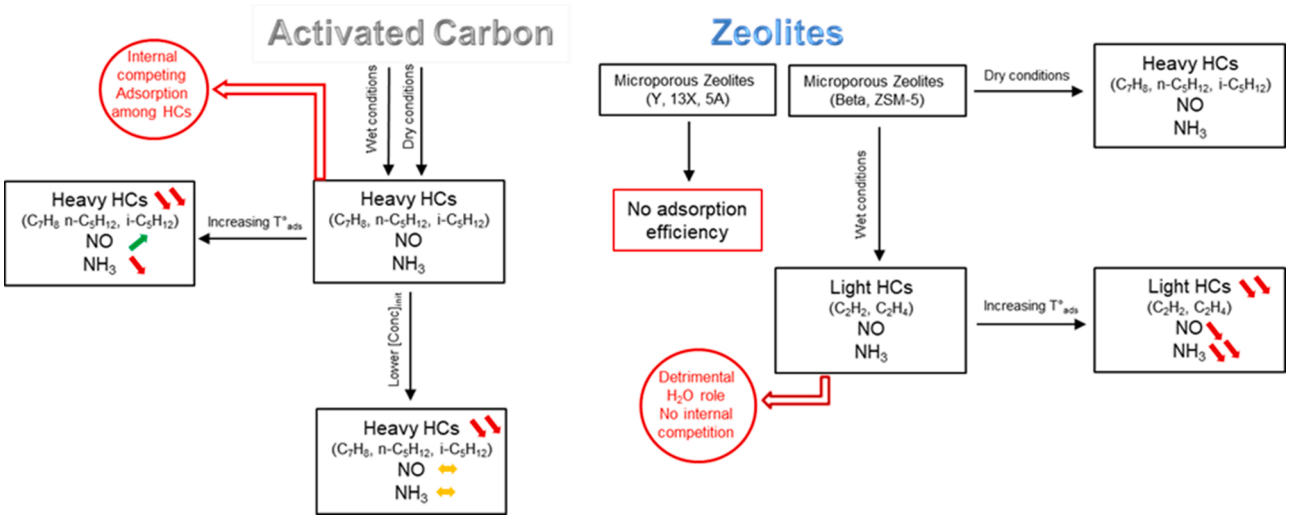

Scheme 3. Schematic overview of cross-effect over all the sorbents. The small arrows indicate the trend in quantitative adsorption of each species upon variation of the parameters under study.

(physical adsorption). In such cases, an increase in temperature triggers changes in the system equilibrium, thereby hindering the retention of gas in the solid sorbent. Whereas, in case of chemisorption, an increase in temperature (above 200 °C) can favor the reaction between the adsorbate and sorbent, thus increasing the adsorption capacity, as reported [47]. However, it should be stressed that the ideal temperature for chemical adsorption is directly dependent on the adsorbate/sorbent system involved.

Guo et al. found that, regardless of the temperature at which adsorption took place, the NH_3 adsorbed over AC (prepared from palm shells) impregnated with sulfuric acid could be divided into two parts: NH_3 (I), physisorbed to the AC surface via weak Van der Waals forces and easily desorbed at the same temperature than for adsorption; and NH_3 (II), chemisorbed to the AC surface via strong hydrogen bonding and could only desorb at a higher temperature of 200 °C. They also found that the adsorptive capacity of chemisorption increased with the amounts of oxygen, which were present in the form of surface oxygen functional groups.

In summary, the good candidate for NH_3 adsorption should be hydrophilic. This state would not only be beneficial for NH_3 adsorption, but complementary and not competitive for the adsorption of light NMHC. Very recently, the beneficial role of H_2O on the low-temperature (< 300 °C) activity of Cu-LTA zeolites in NH_3-SCR was proved. On the basis of the overall DFT calculation results, a new mechanism, where both $[Cu^{I}(H_2O)(NH_3)]^+$ and $[Cu^{I}(NH_3)_2]^+$ complexes are involved as reaction intermediates, is proposed highlighting how water can change the type of intrazeolitic copper species [48]. In our case, the sorbent work upstream an ATS, the analysis of release profile of NH_3 is a key point. The gradual release with temperature, most prevailing at low temperatures range, provides a NH_3 source at the SCR catalytic converter light off, but the temperature desorption > 200 °C avoids boosting the undesired formation of NH_4NO_3, detrimental for the catalyst. It is thus essential to tune the properties of the sorbent to reach a compromise between the two phenomena.

5. Conclusions

The evaluation of different commercial sorbents (sieved powder) has revealed that a solution to reduce exhaust emissions needs a more complex architecture, for example two or more sorbents in series. Moreover, the exhaust line must be adapted using for example a bypass of the sorbents. Analyzing the adsorption capacity of each sorbent showed that capacities are higher at lower temperatures when considering mixtures representative of gasoline engine exhausts. Despite of the complexity of the mixtures, the behavior of single molecule adsorption can be simplified.

Activated Carbon shows a high adsorption capacity towards NMHCs and the highest mass trap efficiency for toluene, and in less extent towards n-pentane and i-pentane. It also seems not to be impacted by the co-feeds of other pollutants, but rather by the temperature of the sorbent and time on stream, during which some competitive adsorption and desorption take place. Moreover, side reactions occur upon heating the sorbent for regeneration.

The other light NMHC molecules such as ethylene and acetylene, as well as ammonia, are mostly retained over Cu-based zeolite, and in particular Cu/ZSM-5, boosted by the presence of water. In dry conditions, only heavy NMHCs are adsorbed on those sorbents. This is an important behavior, as water is always present in exhaust gases.

The release of the retained pollutants occurs at lower temperatures than those at which degradation of the sorbents begins (below than 350 °C and 250 °C for Cu/zeolites and AC, respectively). This suggests the possibility to recover the sorption capacity by reinjecting the flow upstream the ATS, or ii) passing the flow through an 'ozone part', where ozone reacts with the unconverted pollutants. This latter solution may help also in abatement of the other co-fed gases such as CH_4, CO, N_2O which have not been processed. Finally, for NO very low performance was observed whatever the sorbent used and the reaction conditions considered. An overall summary of all the most prominent effects is reported in Scheme 3.

Mass trap efficiency (in view of irreversible desorption) has been evaluated by TPD runs, which provides the temperature ranges suitable for a good synergy with the working temperatures of an ATS system. In this context, the choice of a proper protocol to model adsorption and desorption phase for HCs and NH_3 reflects a good accuracy with experimental data, and that of literature. The model will allow to define the optimal combination of sorbents and their respective volumes in a real exhaust pipeline application.

The promising results for HCs and ammonia storage with material in powder shape will lead to the upgrade in form of monolith to confirm and validate the storage efficiency and capacity. Combined with other technologies, these sorbent materials could be further implemented in a Neutral Air Quality Impact Vehicle (NAQIV) to demonstrate their performance to reduce the engine emissions.

Funding sources

ARAMCO, Saudi Arabia IDs PO#4 provided financial support for the conduct of the research and study design; IFPEN provided the collection and writing of the report. Both supported the analysis, interpretation of data and the decision to submit the article for publication.

CRediT authorship contribution statement

The manuscript was written through the contributions of all authors. All authors have given approval to the final version of the manuscript. **K. Barbera-Italiano:** Data curation, Writing – original draft, Visualization. **E. Jeudy:** Conceptualization, Data curation, Validation, Methodology Writing – review & editing. **M. Lecompte**: Conceptualization. **E. Laigle:** Software, Formal analysis, Writing – review & editing. **C. Norsic**: Conceptualization, Validation, Writing – review & editing. **C. Chaillou:** Project administration, Writing – review & editing. **G. Bourhis**: Project administration, Writing – review & editing.

Declaration of Competing Interest

The authors declare that they have no known competing financial interests or personal relationships that could have appeared to influence the work reported in this paper.

Appendix A. Supplementary material

Supplementary data associated with this article can be found in the online version at doi:10.1016/j.apcatb.2021.120962.

References

[1] T. Johnson, A. Joshi, Review of vehicle engine efficiency and emissions, SAE Int. J. Engines 11 (2018) 1307–1330, https://doi.org/10.4271/2018-01-0329.
[2] K. Mehsein, C. Norsic, C. Chaillou, A. Nicolle, Minimizing secondary pollutant formation through identification of most influential volatile emissions in gasoline exhausts: impact of the vehicle powertrain technology, Atm. Environ. 226 (2020), 117394, https://doi.org/10.1016/j.atmosenv.2020.117394.
[3] D. Shindell, N. Borgford-Parnell, M. Brauer, A. Haines, J.C.I. Kuylenstierna, S. A. Leonard, V. Ramanathan, A. Ravishankara, M. Amann, L. Srivastava, A climate policy pathway for near- and long-term benefits, Science 356 (2017) 493–494, https://doi.org/10.1126/science.aak9521.
[4] J. Lee, J.R. Theis, E.A. Kyriakidou, Vehicle emissions trapping materials: successes, challenges, and the path forward, Appl. Catal. B: Environ. 243 (2019) 397–414, https://doi.org/10.1016/j.apcatb.2018.10.069.
[5] M.V. Twigg, Progress and future challenges in controlling automotive exhaust gas emissions, Appl. Catal. B: Environ. 70 (2007) 2–15, https://doi.org/10.1016/j.apcatb.2006.02.029.
[6] S.B. Kang, S.B. Nam, B.K. Cho, I.-S. Nam, C.H. Kim, S.H. Oh, Effect of speciated HCs on the performance of modern commercial TWCs, Catal. Today 231 (2014) 3–14, https://doi.org/10.1016/j.cattod.2013.11.032.
[7] Z. Sarshar, M.H. Zahedi-Niaki, Q. Huang, M. Eić, S. Kaliaguine, MTW zeolites for reducing cold-start emissions of automotive exhaust, Appl. Catal. B: Environ. 87 (2009) 37–45, https://doi.org/10.1016/j.apcatb.2008.08.025.
[8] SAE Technical Paper Series, SAE International 400 Commonwealth Drive, Warrendale, PA, United States, 2019.
[9] A. Gremminger, J. Pihl, M. Casapu, J.-D. Grunwaldt, T.J. Toops, O. Deutschmann, PGM based catalysts for exhaust-gas after-treatment under typical diesel, gasoline and gas engine conditions with focus on methane and formaldehyde oxidation, Appl. Catal. B: Environ. 265 (2020), 118571, https://doi.org/10.1016/j.apcatb.2019.118571.
[10] A. Iliyas, M.H. Zahedi-Niaki, M. Eić, S. Kaliaguine, Control of hydrocarbon cold-start emissions: a search for potential adsorbents, Microporous Mesoporous Mater. 102 (2007) 171–177, https://doi.org/10.1016/j.micromeso.2006.12.038.
[11] A. Westermann, B. Azambre, Impact of the zeolite structure and acidity on the adsorption of unburnt hydrocarbons relevant to cold start conditions, J. Phys. Chem. C 120 (2016) 25903–25914, https://doi.org/10.1021/acs.jpcc.6b08880.
[12] X. Ye, J.E. Schmidt, R.-P. Wang, I.K. van Ravenhorst, R. Oord, T. Chen, F. de Groot, F. Meirer, B.M. Weckhuysen, Deactivation of Cu-exchanged automotive-emission NH_3-SCR catalysts elucidated with nanoscale resolution using scanning transmission X-ray microscopy, Angew. Chem. Int. Ed. 59 (2020) 15610–15617, https://doi.org/10.1002/anie.201916554.
[13] Jungkuk Lee, Joseph R. Theis, Eleni A. Kyriakidou, Vehicle emissions trapping materials: successes, challenges, and the path forward, Appl. Catal. B: Environ. 243 (2019) 397–414, https://doi.org/10.1016/j.apcatb.2018.10.069.
[14] C. Norsic, G. Bourhis, M. Lecompte, K. Barbera-Italiano, E. Laigle, C. Chaillou, Neutral air quality impact vehicle for urban areas: NMHC and NH_3 adsorption during cold start for ICE based powertrains, in: Proceedings of the THIESEL 2020 Conference on Thermo-and Fluid Dynamics Processes in Direct Injection Engines, 2020. ⟨https://www.researchgate.net/publication/344338201_THIESEL_2020_Conference_on_Thermo-And_Fluid_Dynamic_Processes_in_Direct_Injection_Engines_Neutral_Air_Quality_Impact_Vehicle_for_urban_areas_NMHC_and_NH3_adsorption_during_coldstart_for_ICE_based_pow⟩.
[15] J.D. Pakko, A.A. Adamczyk, W.O. Siegl, R.J. Pawlowicz, Measurements of total and speciated hydrocarbon removal from engine exhaust using activated carbon, SAE Tech. Pap. 941999 (1994), 941999, https://doi.org/10.4271/941999.
[16] S.Y. Bhide, S. Yashonath, n-Pentane and isopentane in one-dimensional channels, J. Am. Chem. Soc. 125 (2003) 7425–7434, https://doi.org/10.1021/ja0285868.
[17] A.M. Carvajal-Bernal, F. Gómez-Granados, L. Giraldo, J.C. Moreno-Piraján, M. Balsamo, A. Erto, Kinetic and thermodynamic study of n-pentane adsorption on activated carbons modified by either carbonization or impregnation with ammonium hydroxide, Microporous Mesoporous Mater. 302 (2020), 110196, https://doi.org/10.1016/j.micromeso.2020.110196.
[18] X. Yang, H. Yi, X. Tang, S. Zhao, Z. Yang, Y. Ma, T. Feng, X. Cui, Behaviors and kinetics of toluene adsorption-desorption on activated carbons with varying pore structure, J. Environ. Sci. 67 (2018) 104–114, https://doi.org/10.1016/j.jes.2017.06.032.
[19] M. Garcia-Oton, F. Montilla, M.A. Lillo-Rodenas, E. Morallon, J.L. Vasquez, Electrochemical regeneration of activated carbon saturated with toluene, J. Appl. Electrochem. 35 (2005) 319–325, https://doi.org/10.1007/s10800-004-7470-3.
[20] J. Wu, L. Zhang, C. Long, Q. Zhang, Adsorption characteristics of pentane, hexane, and heptane: comparison of hydrophobic hypercrosslinked polymeric adsorbent with activated carbon, J. Chem. Eng. Data 57 (2012) 3426–3433, https://doi.org/10.1021/je300550x.
[21] J. Limtrakul, T. Nanok, S. Jungsuttiwong, P. Khongpracha, T.N. Truong, Adsorption of unsaturated hydrocarbons on zeolites: the effects of the zeolite framework on adsorption properties of ethylene, Chem. Phys. Lett. 349 (2001) 161–166, https://doi.org/10.1016/S0009-2614(01)01108-3.
[22] J.P. Wolthuizen, J.P. van den Berg, J.H.C. van Hooff, Low temperature reactions of olefins on partially hydrated zeolite H-ZSM-5, Stud. Surf. Sci. Catal. 5 (1980) 85–92, https://doi.org/10.1016/S0167-2991(08)64868-5.
[23] D. Kalló, G. Onyestyák, Adsorption of acetylene and water on zeolites resulting in hydration to acetaldehyde, Zeolites 17 (1996) 489–494, https://doi.org/10.1016/S0144-2449(96)00074-7.
[24] M. Niwa, N. Katada, New method for the temperature-programmed desorption (TPD) of ammonia experiment for characterization of zeolite acidity: a review, Chem. Rec. 13 (2013) 432–455, https://doi.org/10.1002/tcr.201300009.
[25] V. Dondur, V. Raki, L. Damianovic, A. Auroux, Comparative study of the active sites in zeolites by different probe molecules, J. Serb. Chem. Soc. 70 (2005) 457–474, https://doi.org/10.2298/JSC0503457D.
[26] H. Wang, J. Jia, S. Liu, H. Chen, Y. Wei, Z. Wang, L. Zheng, Z. Wang, R. Zhang, Highly efficient NO abatement over Cu-ZSM-5 with special nanosheet features, Environ. Sci. Technol. 55 (2021) 5422–5434, https://doi.org/10.1021/acs.est.0c08684.
[27] W. Klose, S. Rincón, Adsorption and reaction of NO on activated carbon in the presence of oxygen and water vapour, Fuel 86 (2007) 203–209, https://doi.org/10.1016/j.fuel.2006.06.017.
[28] Y. Li, Y. Guo, T. Zhu, S. Ding, Adsorption and desorption of SO_2, NO and chlorobenzene on activated carbon, J. Environ. Sci. 43 (2016) 128–135, https://doi.org/10.1016/j.jes.2015.08.022.
[29] F. Cao, J. Chen, M. Ni, H. Song, G. Xiao, W. Wu, X. Gao, K. Cen, Adsorption of NO on ordered mesoporous carbon and its improvement by cerium, RSC Adv. 4 (2014) 16281, https://doi.org/10.1039/C4RA01409J (VV).
[30] Z. Zhu, Z. Liu, S. Liu, H. Niu, Adsorption and reduction of NO over activated coke at low temperature, Fuel 79 (2000) 651–658, https://doi.org/10.1016/S0016-2361(99)00192-1.
[31] Y. Li, J.N. Armor, Temperature-programmed desorption of nitric oxide over Cu-ZSM-5, Appl. Catal. 76 (1991) L1–L8, https://doi.org/10.1016/0166-9834(91)80042-U.
[32] Q. Zuo, Y. Xie, J.E., X. Zhu, B. Zhang, Y. Tang, G. Zhu, Z. Wang, J. Zhang, Effect of different exhaust parameters on NO conversion efficiency enhancement of a dual-carrier catalytic converter in the gasoline engine, Energy 191 (2020), 116521, https://doi.org/10.1016/j.energy.2019.116521.
[33] S.A. Dastgheib, H. Salih, T. Ilangovan, J. Mock, NO oxidation by activated carbon catalysts: impact of carbon characteristics, pressure, and the presence of water, ACS Omega 5 (2020) 21172–21180, https://doi.org/10.1021/acsomega.0c02891.
[34] R. Villamaina, U. Iacobone, I. Nova, E. Tronconi, M.P. Ruggeri, L. Mantarosie, J. Collier, D. Thompsett, Mechanistic insight in NO trapping on Pd/Chabazite systems for the low-temperature NO_x removal from diesel exhausts, Appl. Catal. B: Environ. 284 (2021), 119724, https://doi.org/10.1016/j.apcatb.2020.119724.
[35] W.J. Zhang, S. Rabiei, A. Bagreev, M.S. Zhuang, F. Rasouli, Study of NO adsorption on activated carbons, Appl. Catal. B: Environ. 83 (2008) 63–71, https://doi.org/10.1016/j.apcatb.2008.02.003.
[36] S.L. Winkler, J.E. Anderson, L. Garza, W.C. Ruona, R. Vogt, T.J. Wallington, Vehicle criteria pollutant (PM, NOx, CO, HCs) emissions: how low should we go? npj Clim. Atmos. Sci. 1 (2018) https://doi.org/10.1038/s41612-018-0037-5.
[37] T. Steinhaus, M. Thiem, C. Beidl, NO_2-immission assessment for an urban hot-spot by modelling the emission–immission interaction, Automot. Engine Technol. ⟨https://doi.org/10.1007/s41104-021-00080-7⟩.

[38] F. Payri, V.R. Bermúdez, B. Tormos, W.G. Linares, Hydrocarbon emissions speciation in diesel and biodiesel exhausts, Atm. Environ. 43 (2009) 1273–1279, https://doi.org/10.1016/j.atmosenv.2008.11.029.
[39] H.-X. Li, J.M. Donohue, W.E. Chrmier, Y.F. Chu, Application of zeolites as hydrocarbon traps in automotive emission controls, Stud. Surf. Sci. Catal. (2005) 1375–1382.
[40] T. Kanazawa, Development of hydrocarbon adsorbents, oxygen storage materials for three-way catalysts and NOx storage-reduction catalyst, Catal. Today 96 (2004) 171–177, https://doi.org/10.1016/j.cattod.2004.06.119.
[41] N.R. Burke, D.L. Trimm, R.F. Howe, The effect of silica:alumina ratio and hydrothermal ageing on the adsorption characteristics of BEA zeolites for cold start emission control, Appl. Catal. B: Environ. 46 (2003) 97–104, https://doi.org/10.1016/S0926-3373(03)00181-4.
[42] Y. Xi, N.A. Ottinger, Z.G. Liu, Influence of hydrocarbon species on its adsorption on a VSCR catalyst under simulated diesel engine operating conditions, Appl. Catal. B: Environ. 217 (2017) 581–590, https://doi.org/10.1016/j.apcatb.2017.05.077.
[43] I. Heo, S. Sung, M.B. Park, T.S. Chang, Y.J. Kim, B.K. Cho, S.B. Hong, J.W. Choung, I.-S. Nam, Effect of hydrocarbon on DeNOx performance of selective catalytic reduction by a combined reductant over Cu-containing zeolite catalysts, ACS Catal. 9 (2019) 9800–9812, https://doi.org/10.1021/acscatal.9b02763.
[44] Y. Khabzina, D. Farrusseng, Unravelling ammonia adsorption mechanisms of adsorbents in humid conditions, Microporous Mesoporous Mater. 265 (2018) 143–148, https://doi.org/10.1016/j.micromeso.2018.02.011.
[45] J. Valyon, G. Onyestyák, L.V.C. Rees, Study of the dynamics of NH_3 adsorption in ZSM-5 zeolites and the acidity of the sorption sites using the frequency-response technique, J. Phys. Chem. B 102 (1998) 8994–9001, https://doi.org/10.1021/jp981872e.
[46] C.C. Rodrigues, D. de Moraes Jr., S.W. da Nóbrega, M.G. Barboza, Ammonia adsorption in a fixed bed of activated carbon, Bioresour. Technol. 98 (2007) 886–891, https://doi.org/10.1016/j.biortech.2006.03.024.
[47] J. Guo, W.S. Xu, Y.L. Chen, A.C. Lua, Adsorption of NH_3 onto activated carbon prepared from palm shells impregnated with H_2SO_4, J. Colloid Interf. Sci. 281 (2005) 285–290, https://doi.org/10.1016/j.jcis.2004.08.101.
[48] Y. Liu, W. Xue, S. Seo, X. Tan, D. Mei, C.-j. Liu, I.-S. Nam, S.B. Hong, Water: a promoter of ammonia selective catalytic reduction over copper-exchanged LTA zeolites, Appl. Catal. B: Environ. 294 (2021), 120244, https://doi.org/10.1016/j.apcatb.2021.120244.

Further reading

[1] E. Yoda, J.N. Kondo, K. Domen, Detailed process of adsorption of alkanes and alkenes on zeolites, J. Phys. Chem. B 109 (2005) 1464–1472, https://doi.org/10.1021/jp047376.
[2] A. Westermann, B. Azambre, G. Finqueneisel, P. Da Costa, F. Can, Evolution of unburnt hydrocarbons under “cold-start” conditions from adsorption/desorption to conversion: on the screening of zeolitic materials, Appl. Catal. B: Environ. 158–159 (2014) 48–59, https://doi.org/10.1016/j.apcatb.2014.04.005.